Atomic-scale Electronic Structure of the Cuprate Pair Density Wave State Coexisting with Superconductivity

Peayush Choubey[1,2§], Sang Hyun Joo[3§], K. Fujita[4], Zengyi Du[4], S. D. Edkins[5], M. H. Hamidian[6], H. Eisaki[7], S. Uchida[7], A. P. Mackenzie[8], Jinho Lee[3], J.C. Séamus Davis[9,10,11] and P.J. Hirschfeld[12]

1. *Institut für Theoretische Physik III, Ruhr-Universität Bochum, D-44801 Bochum, Germany.*
2. *Department of Physics, Indian Institute of Science, Bengaluru-560012, India.*
3. *Department of Physics and Astron., Seoul National University, Seoul 08826, Korea.*
4. *CMPMS Department, Brookhaven National Laboratory, Upton, NY 11973, USA.*
5. *Department of Applied Physics, Stanford University, Stanford, CA 94305*
6. *Department of Physics, Harvard University, Cambridge MA, USA.*
7. *Inst. of Advanced Industrial Science and Tech., Tsukuba, Ibaraki 305-8568, Japan.*
8. *Max-Planck Institute for Chemical Physics of Solids, D-01187 Dresden, Germany.*
9. *LASSP, Department of Physics, Cornell University, Ithaca NY 14850, USA*
10. *Clarendon Laboratory, University of Oxford, Oxford, OX1 3PU, UK*
11. *Department of Physics, University College Cork, Cork T12 R5C, Ireland*
12. *Department of Physics, University of Florida, Gainesville, FL, USA*

§ *These authors contributed equally to this project.*

The defining characteristic of hole-doped cuprates is *d*-wave high temperature superconductivity. However, intense theoretical interest is now focused on whether a pair density wave state (PDW) could coexist with cuprate superconductivity (D. F. Agterberg *et al., arXiv:*1904.09687 (2019)). Here, we use a strong-coupling mean-field theory of cuprates, to model the atomic-scale electronic structure of an eight-unit-cell periodic, *d*-symmetry form factor, pair density wave (PDW) state coexisting with *d*-wave superconductivity (DSC). From this PDW+DSC model, the atomically-resolved density of Bogoliubov quasiparticle states $\mathbf{N}(\boldsymbol{r},\boldsymbol{E})$ is predicted at the terminal BiO surface of $Bi_2Sr_2CaCu_2O_8$ and compared with high-precision electronic visualization experiments using spectroscopic imaging STM. The PDW+DSC model predictions include the intra-unit-cell structure and periodic modulations of $\mathbf{N}(\boldsymbol{r},\boldsymbol{E})$, the modulations of the coherence peak energy $\boldsymbol{\Delta_p}(\boldsymbol{r})$, and the characteristics of Bogoliubov quasiparticle interference in scattering-wavevector space ($\boldsymbol{q}$ −space). Consistency between all these predictions and the corresponding experiments indicates that lightly hole-doped $Bi_2Sr_2CaCu_2O_8$ does contain a PDW+DSC state. Moreover, in the model the PDW+DSC state becomes unstable to a pure DSC state at a critical hole density p^*, with empirically equivalent phenomena occurring in the experiments. All

these results are consistent with a picture in which the cuprate translational symmetry breaking state is a PDW, the observed charge modulations are its consequence, the antinodal pseudogap is that of the PDW state, and the cuprate critical point at $p^* \approx 19\%$ occurs due to disappearance of this PDW.

Keywords: Cuprate Pseudogap, Pair Density Wave State, Quasiparticle Interference,

Significance Statement:

By making a variety of quantitative comparisons between electronic visualization experiments and a new theory describing coexisting pair density wave and superconductive states in cuprates, we find striking correspondence throughout. Our model can thus explain the microscopic origins of many key atomic-scale phenomena of the cuprate broken-symmetry state. These observations are consistent with the possibility that a short-range pair density wave state coexists with superconductivity below a critical hole-density in $Bi_2Sr_2CaCu_2O_8$, that the charge density wave modulations in cuprates are a consequence of the PDW state, that the cuprate pseudogap is the antinodal gap of the PDW, and that the critical point in the cuprate phase diagram occurs due to disappearance of the PDW.

The Pair Density Wave and Pseudogap States of Cuprates

1 In the elementary undoped CuO_2 plane, each Cu $d_{x^2-y^2}$ orbital is occupied by a single electron and, because the energy required to doubly occupy this orbital is $U \sim 3\ eV$, a Mott insulator (MI) state develops[1,2]. The superexchange spin-spin interaction energy between neighboring $d_{x^2-y^2}$ electrons is $J \sim 150\ meV$, leading to a robust antiferromagnetic (AF) phase[3,4] (Fig 1a). But this AF insulating state vanishes with the removal of as little as 3% of the electrons per Cu site (hole-density p=3%), to reveal the pseudogap (PG) state in a region of the phase diagram bounded by $p < p^*$ and temperatures $T < T^*(p)$ (Fig. 1a). Key characteristics of the PG state include[3,4] a steep drop in both magnetic susceptibility and c-axis conductivity; an apparently incomplete Fermi surface consisting of coherent quasiparticle states on four $\boldsymbol{k}$−space arcs neighboring $\boldsymbol{k} \approx (\pm\pi/2a, \pm\pi/2a)$; an energy gap Δ^* in the spectrum of quasiparticle states near $\boldsymbol{k} \approx (\pm\pi/a, 0); (0, \pm\pi/a)$; and the

depletion of the average density of electronic states $N(E)$ for $|E| < \Delta^*$ where $\Delta^*(p)$ diminishes to zero at $p = p*$ (Fig. 1a). A mean-field energy-gap in the spectrum of coherent $\boldsymbol{k}$-space quasiparticles occurring only near $\boldsymbol{k} \approx (\pm\pi/a\,, 0); (0, \pm\pi/a\,, 0)$ could provide a simple phenomenological explanation for virtually all these PG characteristics, but no comprehensive microscopic theory for the PG phase has yet been established.

2 Extensive evidence has recently emerged for electronic symmetry breaking within the PG phase (Fig. 1a). Bulk probes of charge density find translational symmetry breaking in a density-wave (DW) state with axial wavevectors $\boldsymbol{Q} = (Q, 0); (0, Q)$ parallel to the CuO_2 axes[1,2,5]. Similarly, direct visualization with sub-unit-cell resolution using single-electron tunneling in $Bi_2Sr_2CaCu_2O_8$ and $Ca_{2-x}Na_xCuO_2Cl_2$ reveals intense electronic structure modulations[6,7] that are locally unidirectional[7, 8], exhibit lattice-commensurate periodicity[9,10] for all $p < p*$ [11], have a d-symmetry form factor[8, 12] , and are concentrated at particle-hole symmetric energies[13] $|E| \approx \Delta^*(p)$. The spatial configurations consist of nanoscale regions within which the modulations are commensurate and unidirectional along either[7,8,10,12] $(Q, 0)$ or $(0, Q)$. A complete theoretical explanation for the microscopic origin of these complex atomic-scale electronic structures[6,7,8,9,10,12] has never been elucidated. Figure 1b shows a representative example of $Z(\boldsymbol{r}, E = \Delta) = N(\boldsymbol{r}, +\Delta)\,/N(\boldsymbol{r}, -\Delta)$ for this state at $p \approx 8\%$, along with the simultaneously measured topograph $T(\boldsymbol{r})$ at the BiO layer with the Cu sites indicated by crosses. Figure 1c shows the measured differential tunneling conductance $g(E)$ averaged over the whole FOV of Fig. 1b, and identifies the two characteristic energies Δ_1 and Δ_0. Thus, a key challenge for cuprate studies is to identify microscopically the broken symmetry state in Fig. 1b,c that coexists with the DSC phase and to determine its relationship to the pseudogap.

3 Because the strong electron-electron interactions subtending the MI state persist even when the long-range AF order disappears (Fig. 1a), strong-coupling theory also seems necessary in the PG phase. One frequently recurring consequence[14- 22] of such theories is the existence of a state that breaks translational symmetry by modulating the electron-pairing field as

$$\Delta_1(\boldsymbol{r}) = F_P \Delta_1 \left[e^{iQ_P \cdot r} + e^{-iQ_P \cdot r} \right] \qquad (1)$$

This is a pair density wave state for which Δ_1 is the magnitude of the PDW order parameter and F_P is its form-factor symmetry. Moreover, such a strong-coupling PDW state intertwines[23] the modulations of electron-pair field, of the site/bond charge density, and of spin density. Focus on whether such a PDW state exists in the ground state of cuprates has been further motivated by growing experimental evidence[24-29,30] that is consistent therewith. Obviously, if this PDW state occurs, it must coexist in the $T \to 0$ ground state together with the robust *d*-wave superconductivity (Fig. 1a). Therefore, an urgent research priority is to understand the atomic-scale electronic structure of a PDW coexisting with a DSC state. This is quite challenging because it requires a theoretical description of PDW+DSC electronic structure at the intra-unit-cell scale in $\boldsymbol{r}$-space, and simultaneously throughout a Brillouin zone in $\boldsymbol{k}$-space that is strongly altered by the PDW's existence.

Theory for Cuprate Pair Density Wave and coexisting Superconductivity

4 A classic theory for hole-doped CuO_2 plane electronic structure is based on the *t-J* model, in which electrons hop with matrix element t between Cu $d_{x^2-y^2}$ orbitals, onsite Coulomb energy $U \to \infty$ to completely prevent their double occupancy, resulting in strong antiferromagnetic exchange interactions $J=4t^2/U$. Its Hamiltonian is $H = -\sum_{(i,j),\sigma} P_G t_{ij} (c^\dagger_{i\sigma} c_{j\sigma} + h.c.) P_G + J \sum_{<i,j>} \mathbf{S_i} \cdot \mathbf{S_j}$, where the operator P_G projects out all doubly occupied orbitals from the Hilbert space (Methods A). A renormalized mean-field theory (RMFT) approximation to this *t-J* model is then of great utility in describing the CuO_2 plane physics[31]; it replaces the exact projection P_G operation with renormalization factors g_i^t and g_i^s determine by the average number of charge and spin configurations permissible at every Cu site. The resulting Hamiltonian can be decoupled into a simpler but diagonalizable approximation by using the mean-fields describing on-site hole density δ_i , bond field $\chi_{ij\sigma}$, and electron-pair field $\Delta_{ij\sigma}$ (Methods A). Subsequent variational minimization of the ground state energy with respect to the unprojected wavefunction $|\Psi_0>$ leads to a set of Bogoliubov-de Gennes (BdG) equations, together with self-consistency conditions on the mean fields. To allow breaking of translational symmetry within RMFT, site-specific and

bond-specific renormalization factors $g^t_{i,j}$ and $g^s_{i,j}$ for charge and spin are introduced[17]. To obtain a PDW+ DSC solution, the BdG equations are initialized with a set of order parameter fields modulating at wavevector $\boldsymbol{Q}_P = (1/8,0)2\pi/a_0$, and a self-consistent solution is found. From the consequent many-body wavefunction $\Psi_0(\boldsymbol{r})$ of this broken-symmetry state, the net charge on each Cu site

$$\delta_i = 1 - < \Psi_0 | \sum_\sigma n_{i\sigma} | \Psi_0 > \quad (2)$$

the bond field between adjacent sites *i,j*

$$\chi_{ij\sigma} = < \Psi_0 | c^\dagger_{i\sigma} c_{j\sigma} | \Psi_0 > \quad (3)$$

and the electron-pair field on the bond between adjacent sites *i,j*

$$\Delta_{ij\sigma} = \sigma < \Psi_0 | c_{i\sigma} c_{j\bar{\sigma}} | \Psi_0 > \quad (4)$$

can all be calculated. We note that the commensurate PDW+DSC studied here is not the ground state of the cuprate RMFT Hamiltonian, but that its energy above the homogeneous ground state is so tiny[17,20,21] (~1meV per Cu as discussed in Methods A) that it may be stabilized by a variety of means, including disorder.

Comparison of Pair Density Wave plus Superconductivity Theory with Experiment

5 Using this model, we explore the atomic-scale characteristics of a unidirectional, $\lambda = 8a_0$ PDW state coexisting with uniform DSC. Figure 2a shows the predicted hole density δ_i on the Cu sites exhibiting dominant $\lambda = 4a_0$ modulations, together with the projected *d*-wave superconducting order parameter amplitude Δ_i on the same sites. The corresponding Fourier components of the hole density $\delta(\boldsymbol{q})$ and electron-pair field $\Delta(\boldsymbol{q})$ are shown in Fig. 2b. Here it is important to note that the PDW-induced charge modulation amplitude at $\lambda = 8a_0$ is extremely weak for our standard set of parameters (see caption of Figure 2), whereas the induced charge modulation amplitude at $\lambda = 4a_0$ is dominant. Next, in Fig. 2c, we exhibit the projection of the $8a_0$ periodic charge modulations onto the three symmetry-allowed channels *s, s'* and *d,* utilizing the same definitions as, e.g. in Ref. [12] (see Methods A). The charge distribution over the Cu and O sites is clearly characterized by a pronounced *d*-symmetry form factor (dFF), as has been observed directly in experiments[8,12].

6 For comparison with underdoped $Bi_2Sr_2CaCu_2O_8$ measurements, we next use the RMFT PDW+DSC model and evaluate its quasiparticle states with intra-unit-cell resolution using a Wannier function-based method[21,22]. This is designed to allow quantitative predictions of electronic structure in $\boldsymbol{r}$-space, $\boldsymbol{q}$-space and $\boldsymbol{k}$-space of a PDW+DSC state. The band structure parameterization is t=400meV, t'=-0.3t and J=0.3t, all representing $Bi_2Sr_2CaCu_2O_8$ at $p \approx 0.08$. For this parameter set, we calculate the quasiparticle Greens functions in the self-consistently obtained PDW+DSC state, with the unidirectional PDW wavevector $\boldsymbol{Q_P} = (1/8,0)2\pi/a_0$ that is modulating parallel to the x-axis but lattice-periodic along the y-axis, and find the PDW spectral gap $\Delta_1 \approx 0.3t \approx 100meV$, and gap associated with uniform DSC $\Delta_0 \approx 0.07t \approx 25meV$ (Methods A). Moreover, while all previous RMFT studies of cuprates yield only the Cu Site-specific Greens function matrix $G_{ij\sigma}(E)$ within the CuO_2 plane, the experimental measurements of electron-tunneling probability are actually made at a continuum of locations just above the crystal termination BiO layer of $Bi_2Sr_2CaCu_2O_8$ (Fig. 1b). Therefore, we use first-principles Cu $d_{x^2-y^2}$ Wannier functions $W_i(\boldsymbol{r})$ to make quantitative predictions of the $\boldsymbol{r}$-space Green's functions $G_\sigma(\boldsymbol{r},E) = \sum_{ij} G_{ij\sigma}(E) W_i(\boldsymbol{r}) W_j^*(\boldsymbol{r})$ of a PDW+DSC state, everywhere at a height 0.4nm above BiO terminal plane[32,33] (Methods B). We emphasize that none of the mean fields δ_i, $\chi_{ij\sigma}$ and $\Delta_{ij\sigma}$ are related simply to the local quasiparticle density of states $N(\boldsymbol{r},E) = \sum_\sigma -\frac{1}{\pi} \mathrm{Im}\, G_\sigma(\boldsymbol{r},E)$, which must instead be determined from the Bogoliubov quasiparticle eigenstates[20,21,24,25,28,34,35,36] that enter the lattice Green's function $G_{ij\sigma}$. Fig. 2d shows the theoretical $N(\mathbf{r},E)$ for the DSC+PDW state at various points in the modulated state, as identified in the inset. Note that a shoulder-like feature is present at nearly identical particle-hole symmetric energies $\pm\Delta_0$ for all Cu sites, such that we associate it with the uniform d-wave superconducting condensate DSC. By contrast, this model predicts that the energy Δ_p at which the "coherence peak" occurs ($\omega > 0$) varies from atom to atom in real space; its largest magnitude may be associated with the PDW amplitude Δ_1.

7 The bias dependence of $Z(\boldsymbol{r},E) = N(\boldsymbol{r},+E)\,/N(\boldsymbol{r},-E)$ from our PDW+DSC model are then predicted for comparison with experiment. Figure 3a-f shows these $Z(\boldsymbol{r},E)$ data

focusing on the energy range $0.5\Delta_1 \lesssim E \lesssim 1.5\Delta_1$, within which they exhibit a comprehensive *d*-symmetry form factor (Methods B). This effect can be seen directly because the model $Z(\boldsymbol{r}, E)$ has intra-unit-cell precision. Consider the three sublattices making up the primary features of the $Z(\boldsymbol{r}, E)$ image: $Cu(\boldsymbol{r}, E)$ containing only $Z(\boldsymbol{r}, E)$ at copper sites and $O_x(\boldsymbol{r}, E)$ and $O_y(\boldsymbol{r}, E)$, containing only $Z(\boldsymbol{r}, E)$ at the *x*/*y*-axis oxygen sites. By definition, in a *d*-symmetry form factor charge density wave, modulations on the $O_x(\boldsymbol{r}, E)$ and $O_y(\boldsymbol{r}, E)$ sites are out of phase by π. In our PDW+DSC model, such phenomena occur at both $\boldsymbol{Q_P}$ and $\boldsymbol{2Q_P}$, first appear near $E \approx \Delta_1/2$, are intense surrounding $E \approx \Delta_1$ and eventually disappear near $E \approx 2\Delta_1$ (Methods B and Ref. 8). This energy dependence, including both the dominance of the dFF in a wide range of energies surrounding Δ_1, as well as the low-energy dominance of the *s'* form factor, were demonstrated earlier using the same theory[21] but for an incommensurate wavevector.

8 For experimental comparison with our PDW+DSC model, we visualize the electronic structure[37] using spectroscopic imaging STM (SISTM) measurements of STM-tip-sample differential electron tunneling conductance $dI/dV(\boldsymbol{r}, V) \equiv g(\boldsymbol{r}, V)$. We study the terminal BiO layer of $Bi_2Sr_2CaCu_2O_8$ for a range of tip-sample voltage differences *V* and at T=4.2K. In theory, $g(\boldsymbol{r}, V) \propto N(\boldsymbol{r}, E)/\int_0^{eV_s} N(\boldsymbol{r}, E)dE$ (V_s is the junction-formation voltage). The ratio $Z(\boldsymbol{r}, E) = g(\boldsymbol{r}, +V)/g(\boldsymbol{r}, -V)$ is widely used in such visualization studies because, even if $\int_0^{eV_s} N(\boldsymbol{r}, E)dE$ is heterogeneous, it yields a valid measure of periodicities and broken symmetries[37]. Figures 3g-l show the measured $Z(\boldsymbol{r}, E)$ in the energy range $0.5\Delta_1 \lesssim E \lesssim 1.5\Delta_1$, with each panel shown side-by-side with the equivalent energy in the model. The most intense modulations occur at $E \approx \Delta_1(p)$ for all $p < 0.19$ (Ref.8, 13), and all through this energy range they exhibit a comprehensive *d*-symmetry form factor[8,12,13]. Therefore, correspondence between theoretical $Z(\boldsymbol{r}, E)$ from the PDW+DSC model (Fig. 3a-f) and the measured $Z(\boldsymbol{r}, E)$ (Fig. 3g-l) is observed to be excellent over a wide energy range. This can be quantified by measuring the cross-correlation value of each pair of theory: experiment

$Z\left(\boldsymbol{r}, E/\Delta_1\right)$ images . The result, shown in Fig. 3m, demonstrates strong cross-correlations between theory-experiment pairs of $Z(\boldsymbol{r}, E)$ images throughout the energy range. Therefore, predictions of PDW+DSC theory, on distance scales ranging from $8a_0$ down to sub-unit cell, corresponds strongly and in detail to the complex patterns of quasiparticle states observed in the broken symmetry state of $p<p^*$ $Bi_2Sr_2CaCu_2O_8$.

9 Next, as seen in Fig. 2d, the theory predicts that coherence peak energy Δ_p varies substantially from one unit cell to the next within the $\lambda = 8a_0$ PDW. In Fig. 4a we show the theoretical gap map for the PDW+DSC state obtained by identifying the coherence peak energy $\Delta_p(r)$ for ω>0 at all intra-unit cell points over an area of 8x12 unit cells, while Fig. 4b shows the gap map obtained by using the same algorithm to determine $\Delta_p(r)$ from measured dI/dV spectra. Both theory and experiment show $8a_0$ periodic $\Delta_p(r)$ modulations within which there are smaller atomically resolved variations that exhibit common characteristics but are not identical, most likely because of inadequacies in the DFT-derived Wannier functions in representing underdoped cuprates.

10 Finally, we consider the effects of a PDW+DSC state on Bogoliubov quasiparticle scattering interference[38] (BQPI)**.** This occurs when an impurity atom scatters quasiparticles, which then interfere to produce characteristic modulations of $N(\boldsymbol{r}, E)$ surrounding each impurity atom. Local maxima in $Z(\boldsymbol{q}, E)$, the power-spectral-density Fourier transform of $Z(\boldsymbol{r}, E)$, reveal the sets of energy dispersive wavevectors $\boldsymbol{q}_i(E)$ generated by the scattering interference[11]. A BQPI data set thus consists of a sequence of $Z(\boldsymbol{q}, E)$ images spanning the energy range of interest, from which an efficient synopsis over all the QPI modulations can be achieved[11] using $\Lambda(\boldsymbol{q}, \Delta) = \sum_{E=0}^{\Delta} Z(\boldsymbol{q}, E)$. The key utility here is that $\Lambda(\boldsymbol{q}, \Delta)$ provides an efficient and characteristic "fingerprint" of whatever ordered state(s) controls the $\boldsymbol{q}_i(E)$ of the BQPI processes. For our PDW+DSC model, we calculate $Z(\boldsymbol{q}, E)$ using a simple point-like scatterer within the RMFT framework (Methods C). From these model $Z(\boldsymbol{q}, E)$ images, the predicted $\Lambda(\boldsymbol{q}, \Delta_0) = \sum_{E=0}^{\Delta_0} Z(\boldsymbol{q}, E)$ is determined and shown in Fig. 5a. This contains the overall $\Lambda(\boldsymbol{q}, \Delta_0)$ fingerprint expected of the BQPI in this PDW+DSC state. For comparison, Fig.

5b includes the predicted $\Lambda(\boldsymbol{q}, \Delta_0)$ of a simple *d*-wave superconductor with a Fermi surface at p=23%. It reflects the familiar peaks characteristic of dispersing Bogoliubov quasiparticles, including the tracing of the Fermi surface by the peak conventionally labelled $\boldsymbol{q}_4$ as bias voltage is varied[11]. Clearly, the PDW+DSC $\Lambda(\boldsymbol{q}, \Delta_0)$ in Fig 5a is very different, exhibiting very weak dispersion and thus producing sharper $\boldsymbol{q}$-space spots, as well as the absence of any $\boldsymbol{q}_4$ scattering interference near edges of $\boldsymbol{q}$-space reciprocal unit cell. To compare these predictions for $\Lambda(\boldsymbol{q}, \Delta_0)$ with and without the PDW order to experiments, we show measured $\Lambda(\boldsymbol{q}) = \sum_{E\cong 0}^{\Delta_0} Z(\boldsymbol{q}, E)$ for both low p and high p in Fig. 5c,d. The very distinct characteristics of $\Lambda(\boldsymbol{q}, \Delta_0)$ observed at low p and high p, are in striking agreement with the PDW+DSC model predictions for $\Lambda(\boldsymbol{q}, \Delta_0)$ with and without the PDW state respectively. Moreover, the empirical BQPI phenomena in Fig. 5c are a characteristic of the pseudogap region of the phase diagram[11] whereas the PDW+DSC model that predicts them (Fig. 5a) does not require a separate pseudogap to be introduced because the $\boldsymbol{k}$-space structure of the PDW is what gaps antinodes[34]. Finally, in our PDW+DSC model, we find that increasing p leads to an instability of the PDW order towards a uniform DSC state via a weak first order transition at $p \approx 0.18$ (Methods A), whereas the experimentally observed disappearance of translational symmetry breaking simultaneous with the reappearance of low energy quasiparticles at the antinodes[11], occurs at $p \approx 0.19$.

Pair Density Wave plus Superconductivity Theory and Other Techniques

11 We note that NMR and XRAY studies (primarily of $YBa_2Cu_3O_7$ and La_2BaCuO_4)[39] appear consistent with SISTM visualizations of incommensurate electronic density modulations (primarily of $Bi_2Sr_2CaCu_2O_8$ and $Ca_{2-x}Na_xCuO_2Cl_2$)[37], and to have a common microscopic cause[40,41]. But in our current study, we have compared carefully to atomic scale studies of $Bi_2Sr_2CaCu_2O_8$ that manifest short-range commensurate periodicity in electronic structure images[7,9,10,12]. These two phenomenologies may appear mutually contradictory. However, the XRAY and Fourier transform STM (FTSTM) studies focus only on a specific wavevector, and this procedure discards all the other information distributed throughout $\boldsymbol{q}$-space. In $Bi_2Sr_2CaCu_2O_8$, that data actually contains the extremely complex information on the effects of form factor symmetry, and on how the commensurate, unidirectional

electronic-structure patters proliferate throughout real-space[10]. Thus, the coexistence of a local maximum at incommensurate wavevector in XRAY or FTSTM measurements, with commensurate electronic structures distributed throughout real space, is a demonstrable characteristic of $Bi_2Sr_2CaCu_2O_8$ electronic structure[10]. The most likely resolution is that the measured incommensurate behavior in XRAY or FTSTM experiments represent really *discommensurate* behavior, where commensurate, unidirectional DW are coupled by random phase slips. Indeed, by using advanced techniques, these phase slips are identifiable directly in the N($\boldsymbol{r}$,E) modulations of $Bi_2Sr_2CaCu_2O_8$ (Ref. 9). Another interesting and related issue is the existence or nonexistence of an XRAY scattering peak at $\boldsymbol{Q} = 2\pi/a_0(1/8,0)$, because this is one of the indications that that CDW modulations are induced by $\lambda = 8a_0$ PDW order in the presence of DSC. Although such a peak has been observed for N($\boldsymbol{r}$,E) both within vortex halos[42] and at zero-field in $Bi_2Sr_2CaCu_2O_8$, attempts to detect it by XRAY measurements on $YBa_2Cu_3O_7$ at zero-field have not yet succeeded. Importantly, one of the surprises of our PDW+DSC model is that only a tiny $\boldsymbol{Q} = 2\pi/a_0(1/8,0)$ charge modulation peak is predicted (black in Fig. 2b), whose intensity may be below present XRAY detection limits. Alternatively, the PDW in $YBa_2Cu_3O_7$ may be fluctuating and thus unobservable[43]. A distinct point is that a uniform DSC+PDW state should have clear spectroscopic signatures visible in angle-resolved photoemission (ARPES)[24,28]. And, to first order, the PDW+DSC model and ARPES correspond well, because the strong antinodal gap due to the PDW is empirically indistinguishable from the antinodal "pseudogap" reported by virtually all ARPES studies. But some fine features the PDW+DSC model predicts for $A(\boldsymbol{k},\omega)$ have not yet been seen by ARPES, presumably due to the short-range nature of the static PDW+DSC patches. Future theoretical modeling studies of disordered PDWs will be necessary to explore these issues. Finally, one may wonder whether a $4a_0$ periodic CDW state coexisting with a *d*-wave superconductor could reproduce the N($\boldsymbol{r}$,E) data or the QPI signatures as well as our PDW+DSC model. In that regard, we find that one must initialize the RMFT equations with a modulating pair-field to obtain a non-uniform state and that any other type of initialization, for example a $4a_0$ periodic CDW, converges only to uniform DSC. More generally, Ginzburg-Landau models based on a large DSC order parameter coexisting with a CDW of wavevector $\boldsymbol{Q}_{CDW}$ (and possibly an induced PDW at $\boldsymbol{Q}_{CDW}$), do not have PDW at $\boldsymbol{Q}_{CDW}/2$. Thus, experimentally, the presence of $8a_0$ periodic

modulations along with a particle-symmetric kink at low energies, favor the PDW+DSC interpretation.

Discussion and Conclusions

12 To recapitulate, we have developed a strong-coupling mean-field theory for a coexisting *d*-wave superconductor and pair density wave ($\lambda = 8a_0$) and made detailed comparisons of its predictions with experimental SISTM data from $Bi_2Sr_2CaCu_2O_8$. To allow valid quantitative comparison to such experiments, the atomic-scale tunneling characteristics of the PDW+DSC state at the BiO termination layer of the crystal were predicted utilizing a recently developed Wannier-function based method. Then, from the $8a_0$ scale down to inside the CuO_2 unit cell, we find that the predictions (Fig. 2a-d, Fig. 3a-f) correspond strikingly well with the highly complex electronic structure patterns observed by SISTM (Fig. 3g-l) in the $p<p^*$ broken-symmetry state of $Bi_2Sr_2CaCu_2O_8$. Indeed, the PDW+DSC model explains simply the microscopic origins of many enigmatic characteristics of this broken-symmetry state, including the $\lambda = 4a_0$ *d*-symmetry form factor $N(\boldsymbol{r}, E)$ modulations[6-10,12] and the concentration of their amplitude maxima[8,9,12,13] surrounding $|E| = \Delta_1$. Further, by considering scattering of $\boldsymbol{k}$-space quasiparticles, we explore the QPI "fingerprint" $\Lambda(\boldsymbol{q}, \Delta_0)$ of the PDW+DSC model (Fig. 5a), and find it too in strong, detailed agreement with measured $\Lambda(\boldsymbol{q}, \Delta_0)$ (Fig. 5c). Hence, the antinodal pseudogap that dominates the experimental data $\Lambda(\boldsymbol{q}, \Delta_0)$ (Fig. 5c) plausibly corresponds to the antinodal gap of the PDW in the model $\Lambda(\boldsymbol{q}, \Delta_0)$ (Fig. 5a). Further, the transition at $p \approx 18\%$ in the model from the $\Lambda(\boldsymbol{q}, \Delta_0)$ characteristic of a PDW+DSC state (Fig. 5a) to that of a pure d-wave superconductor (Fig. 5b) corresponds qualitatively with the experimentally observed[11] transition in $\Lambda(\boldsymbol{q}, \Delta_0)$ at $p \approx p*$ (Fig. 5c,d). Consequently, the disappearance at a critical hole-density p^* of both the $\boldsymbol{r}$-space symmetry-breaking structures (Fig. 3a-f) and the concomitant $\boldsymbol{q}$-space QPI signatures (Fig. 5c) are all features that occur in the PDW+DSC model at the hole-density where the PDW disappears. Overall, the agreement between our PDW+DSC model and the plethora of experimental characteristics is consistent with a picture in which a disordered $\lambda = 8a_0$ PDW+DSC state exists for $p < p*$ in $Bi_2Sr_2CaCu_2O_8$, the $\lambda = 4a_0$ charge modulations

observed by XRAY scattering[5,39] are a consequence of this state, the cuprate pseudogap coincides with the antinodal gap of the coexisting PDW, and the cuprate $p \approx p^*$ critical point is due to disappearance of the PDW.

Acknowledgements: The authors acknowledge and thank D. Agterberg, E.-A. Kim, M. Norman, S.A. Kivelson and Y. Wang for very helpful discussions and advice. P.C. and P.J.H. acknowledge support from NSF-DMR-1849751. P.C. acknowledges the research grant PDF/2017/002242 from SERB, DST, India. S.U. and H.E. acknowledge support from a Grant-in-aid for Scientific Research from the Ministry of Science and Education (Japan) and the Global Centers of Excellence Program for Japan Society for the Promotion of Science. S.H.J. and J.L. acknowledge support from the Institute for Basic Science in Korea (Grant No. IBS-R009-G2), the Institute of Applied Physics of Seoul National University, National Research Foundation of Korea (NRF) grant funded by the Korea government (MSIP) (No. 2017R1A2B3009576). S.H.J. also acknowledges support from the BK21 Plus Project. K.F. and Z.D. acknowledge support from the U.S. Department of Energy, Office of Basic Energy Sciences, under contract number DEAC02-98CH10886; J.C.S.D. acknowledges support from the Moore Foundation's EPiQS Initiative through Grant GBMF4544, from Science Foundation Ireland under Award SFI 17/RP/5445 and from the European Research Council (ERC) under Award DLV-788932.

Author Contributions: P.C., P.J.H and J.C.S.D. designed the project. S.H.J., Z.D., S.D.E., M.H.H., J.L. and K.F. carried out the experiments and data analysis. H.E. and S.U. synthesized samples. P.C. and P.J.H carried out theoretical analysis. J.C.S.D. and P.J.H supervised the investigation and wrote the paper with key contributions from P.C., S.H.J. and K.F. The manuscript reflects the contributions of all authors.

Author Information Reprints and permissions information is available at www.nature.com/reprints. The authors declare no competing financial interests. Readers are welcome to comment on the online version of the paper. Correspondence and requests for materials should be addressed to P.J.H and J.C.S.D.

FIGURE CAPTIONS

FIG. 1 Broken-symmetry Phase Coexisting with Cuprate Superconductivity

a) Schematic phase diagram of lightly hole-doped CuO_2. The Mott insulator phase with long range antiferromagnetic order disappears quickly with increasing hole doping *p* to be replaced by the pseudogap phase (PG). The d-wave superconductivity (DSC) coexists with PG phase below some critical hole density p*, and persists as a unique state at p>p*. Within the PG phase, the DW modulations have been reported.

b) Measured $Z(\boldsymbol{r},E=\Delta_1)$ at the BiO termination layer of $Bi_2Sr_2CaCu_2O_8$ for p≈0.1 The locations of Cu atoms of the CuO_2 plane in the same field of view are shown on the topograph T(r) above it.

c) Measured differential conductance averaged over the same field of view as b. The black, dashed lines identify two characteristic energies Δ_1 and Δ_0.

FIG. 2 Characteristic features of our model for a unidirectional PDW+DSC state

(a) Variation of hole density (δ) and d-wave gap order parameter (Δ) with lattice sites i as obtained from the self-consistent solution of the extended t-J model for parameter set doping *x*=0.125,next nearest neighbor (NNN) hopping *t'* = -0.3, exchange interaction *J*=0.3, and temperature T=0.04. Energy scale is presented in units of nearest-neighbor (NN) hopping *t*.

(b) Variation of hole density (δ) and d-wave gap order parameter (Δ) with wavevector $\boldsymbol{q}$ obtained by Fourier transforming corresponding lattice-space quantities shown in (a). Hole density and gap order parameter show largest modulating components at $|\boldsymbol{q}| = 0.25$ and $|\boldsymbol{q}| =0.125$, respectively. But the predicted $|\boldsymbol{q}| =0.125$ component of charge density modulation δ(q) is extremely small, due to the small uniform component of the gap order parameter. Wavevectors are presented in units of $2\pi/a_0$, where a_0 is the lattice constant in the CuO_2 a-b plane.

(c) Density wave form-factors obtained from the hole-density and NN bond order parameter (χ). The d-symmetry form factor is dominant at all wavevectors, with predominant intensity at $|\boldsymbol{q}|=0.25$.

(d) Continuum local density of states N(r,E) at Cu positions along Cu-O_x direction over a period of PDW ($8a_0$). Here $\Delta_1 \approx 0.3$ and $\Delta_0 \approx 0.07$ correspond to the gap-scale associated with the PDW component and uniform DSC component of the PDW+DSC state, respectively.

FIG 3. $Z(\boldsymbol{r},\omega)$ in PDW+DSC state compared to corresponding experimental data

(a)-(f) Predicted $Z(\boldsymbol{r},\omega)$ maps in PDW+DSC state for the terminal BiO layer, at energies $|\omega|=0.4\Delta_1, 0.6\Delta_1, 0.8\Delta_1, \Delta_1, 1.2\Delta_1,$ and $1.4\Delta_1$, respectively.

(g)-(i) Experimentally measured $Z(\boldsymbol{r},E/\Delta_1)$ maps at the terminal BiO layer, for bias voltages corresponding to energies in (a)-(f), respectively.

(m) Cross-correlation coefficient between theoretical $Z(\boldsymbol{r},\omega)$ images and experimental $Z(\boldsymbol{r},E/\Delta_1)$ map images as a function of energy/voltage, showing very strong correspondence between them in the region ($0.5\Delta_1$ -$1.5\Delta_1$, marked with vertical black dashed lines) around PDW energy gap scale. Direct examination of a typical pair, for example (e) and (k), show why the cross correlation coefficient is so high. A wide variety of minute details, including the distinct broken rotational symmetry inside each specific CuO_2 unit cell, the *d*-symmetry modulations of this broken symmetry over eight unit cells, and the bond-centered register of this $8a_0$ unit to the CuO_2 lattice, correspond strikingly between experiment and theory.

FIG. 4 Gapmap $\boldsymbol{\Delta_p(r)}$ derived from coherence-peak energy in PDW+DSC state

(a) Gapmap in PDW+DSC state obtained by identifying coherence peak energy $\Delta_p(\boldsymbol{r})$ for $\omega>0$ at all intra-unit cell points over an area of 8x12 unit cells. Colorbar is given in the units of 't'.

(b) Gapmap $\Delta_p(\boldsymbol{r})$ obtained by following the same procedure as in (a), but for experimentally measured g(r,V) spectra of a representative domain as shown.

(c) Gap $\Delta_p(\boldsymbol{r})$ averaged along y-direction (black) obtained in the PDW+DSC model.

(d) Gap $\Delta_p(\boldsymbol{r})$ averaged along y-direction (black) obtained from the g(r,V) spectra.

FIG 5. Comparison of $\boldsymbol{\Lambda(q,\Delta_0)}$ predictions/data in PDW+DSC and pure DSC states

(a) Predicted $\boldsymbol{\Lambda(q,\Delta_0)}$ map in PDW+DSC state at doping x=0.125.

(b) Predicted $\boldsymbol{\Lambda(q,\Delta_0)}$ map in a uniform d-wave superconductor state at doping x=0.23.

(c) Experimental $\boldsymbol{\Lambda(q,\Delta_0)}$ map for underdoped $Bi_2Sr_2CaCu_2O_8$ at p=0.08$\pm$0.1. In principle $\mathbf{T}(\boldsymbol{q}, \mathrm{eV} = \boldsymbol{\Delta_0})$, the Fourier transform of a topographic image $\mathbf{T}(\boldsymbol{r}, \mathrm{eV} = \boldsymbol{\Delta_0})$**,** would be logarithmically sensitive to the same information as $\boldsymbol{\Lambda(q,\Delta_0)}$. But because it also contains such intense signals from a variety of other phenomena, is has proven difficult to use that approach for QPI studies.

(d) Experimental $\boldsymbol{\Lambda(q,\Delta_0)}$ map for overdoped $Bi_2Sr_2CaCu_2O_8$ at p=0.23.

References

1 B. Keimer, S. A. Kivelson, M. R. Norman, S. Uchida, and J. Zaanen, From quantum matter to high temperature superconductivity in copper oxides. *Nature* **518**, 179-186 (2015).

2 R. Comin and A. Damascelli, Resonant X-ray scattering studies of charge order in cuprates. *Annu. Rev. Condens. Matter Phys.* **7**, 369-405 (2016).

3 M. R. Norman, D. Pines, C. Kallin, The pseudogap: friend or foe of high T_C? *Adv. Phys.* **54**, 715-733 (2005).

4 P. A. Lee, N. Nagaosa and X. -G. Wen, Doping a Mott insulator: Physics of high-temperature superconductivity *Rev. Mod. Phys.* **78,** 17 (2006).

5 A. Frano *et al* Charge Ordering in Superconducting Copper Oxides J. Phys.: Condens. Matter in press https://doi.org/10.1088/1361-648X/ab6140

6 T. Hanaguri *et al*., A 'checkerboard' electronic crystal state in lightly hole-doped $Ca_{2-x}Na_xCuO_2Cl_2$ *Nature* **430**, 1001-1005 (2004).

7 Y. Kohsaka *et al*., An Intrinsic bond-centered electronic glass with unidirectional domains in underdoped cuprates. *Science* **315**, 1380-1385 (2007).

8 M. H. Hamidian *et al*., Atomic-scale electronic structure of the cuprate d-symmetry form factor density wave state. *Nat. Phys.* **12**, 150-156 (2015).

9 A. Mesaros *et al*., Commensurate $4a_0$-period charge density modulations throughout the $Bi_2Sr_2CaCu_2O_{8+x}$ pseudogap regime. *Proc. Nat. Acad. Sci.* **113**, 12661-12666 (2016).

10 Y. Zhang *et al*., Machine learning in electronic-quantum-matter imaging experiments. *Nature* **570**, 484-490 (2019).

11 K. Fujita *et al*., Simultaneous transitions in cuprate momentum-space topology and electronic symmetry breaking. *Science* **344***,* 612-616 (2014).

12 K. Fujita *et al*., Direct phase-sensitive identification of a d-form factor density wave in underdoped cuprates. *Proc. Nat. Acad. Sci.* **111**, E3026-E3032 (2014).

13 S. Mukhopadhyay *et al*., Evidence for a vestigial nematic state in the cuprate pseudogap phase. *Proc. Nat. Acad. Sci.* **116**, 13249-13254 (2019).

14 A. Himeda, T. Kato, and M. Ogata, Stripe states with spatially oscillating *d*-wave superconductivity in the two-dimensional *t*-*t*'-*J* model. *Phys. Rev. Lett.* **88**, 117001 (2002).

15 M. Raczkowski *et al*., Unidirectional *d*-wave superconducting domains in the two-dimensional *t-J* model. *Phys. Rev. B* **76**, 140505 (2007).

16 E. Berg *et al*., Dynamical layer decoupling in a stripe-ordered high-T_C superconductor. *Phys. Rev. Lett.* **99***,* 127003 (2007).

17 K.-Y. Yang, W. Q. Chen, T. M. Rice, M. Sigrist, and F.-C. Zhang, Nature of stripes in the generalized *t–J* model applied to the cuprate superconductors. *New J. Phys.* **11**, 055053 (2009).

18 F. Loder, S. Graser, A. P. Kampf, and T. Kopp, Mean-field pairing theory for the charge-stripe phase of high-temperature cuprate superconductors. *Phys. Rev. Lett.* **107**, 187001 (2011).

19 P. Corboz, T. M. Rice, and M. Troyer, Competing states in the *t-J* model: Uniform d-wave state versus stripe state. *Phys. Rev. Lett.* **113**, 046402 (2014).

20 W.-L. Tu and T.-K Lee, Genesis of charge orders in high temperature superconductors. *Sci. Rep.* **6**, 18675 (2016).

21 P. Choubey, W.-L. Tu, T.-K Lee and P. J. Hirschfeld, Incommensurate charge ordered states in the *t–t'–J* model. *New J. Phys.* **19**, 013028 (2017).

22 S. Verret, M. Charlebois, D. Sénéchal, and A.-M. S. Tremblay, Subgap structures and pseudogap in cuprate superconductors: Role of density waves. *Phys. Rev. B* **95**, 054518 (2017).

23 E. Fradkin, S. A. Kivelson, and J. M. Tranquada. Colloquium: Theory of intertwined orders in high temperature superconductors. *Rev. Mod. Phys.* 87, 457 (2015)

24 P. A. Lee, Amperean pairing and the pseudogap phase of cuprate Superconductors. *Phys. Rev. X* **4,** 031017 (2014).

25 Q. Li, M. Hücker, G. D. Gu, A. M. Tsvelik, and J. M. Tranquada, Two-dimensional superconducting fluctuations in stripe-ordered $La_{1.875}Ba_{0.125}CuO_4$. *Phys. Rev. Lett.* **99**, 067001 (2007).

26 E. Berg, E. Fradkin, and S. A. Kivelson, Charge-4e superconductivity from pair-density-wave order in certain high-temperature superconductors. *Nat. Phys.* **5,** 830-833 (2009).

27 E. Berg, E. Fradkin, S. A. Kivelson, and J. M. Tranquada, Striped superconductors: how spin, charge and superconducting orders intertwine in the cuprates. *New J. Phys.* **11,** 115004 (2009).

28 M. R. Norman and J. C. Seamus Davis, Quantum oscillations in a biaxial pair density wave state. *Proc. Nat. Acad. Sci.* **115**, 5389-5391 (2018).

29 M. H. Hamidian *et al*., Detection of a Cooper-pair density wave in $Bi_2Sr_2CaCu_2O_{8+x}$. *Nature* **532**, 343-347 (2016).

30 S.D. Edkins *et al*., Magnetic-field Induced Pair Density Wave State in the Cuprate Vortex Halo *Science* **364, 976-980** (2019).

31 F. C. Zhang, C. Gross, T. M. Rice, and H. Shiba, A renormalised Hamiltonian approach to a resonant valence bond wavefunction. *Supercond. Sci. Technol.* **1**, 36 (1988).

32 P. Choubey *at al*, Visualization of atomic scale phenomena in superconductors: application to FeSe, Phys Rev. B***90***, 134520 (2014)

33 P. Choubey, A. Kreisel, T. Berlijn, B. M. Andersen, and P. J. Hirschfeld, Universality of scanning tunneling microscopy in cuprate superconductors. *Phys. Rev. B* **96,** 174523 (2017).

34 S. Baruch and D. Orgad, Spectral signatures of modulated *d*-wave superconducting phases. *Phys. Rev. B.* **77**, 174502 (2008).

35 Y. Wang, D.F. Agterberg and A. Chubukov, Coexistence of charge-density-wave and pair-density-wave orders in underdoped cuprates *Phys. Rev. Lett.* **114**, 197001 (2015).

36 W. –L. Tu and T. –K. Lee, Evolution of pairing orders between pseudogap and superconducting phases of cuprate superconductors. *Sci. Rep.* **9**, 1719 (2019).

37 K. Fujita *et al*., Spectroscopic imaging STM: Atomic-scale visualization of electronic structure and symmetry in underdoped cuprates. Strongly correlated systems - Experimental Techniques, Springer Series in Solid-State Sciences (Springer, Berlin), Vol 180, pp 73–109.

38 Q.-H. Wang and D.-H. Lee, Quasiparticle scattering interference in high-temperature superconductors. *Phys. Rev. **B*** **67**, 020511(R) (2003).

39 H. Miao *et al*., Formation of incommensurate charge density waves in cuprates. *Phys. Rev. X* **9**, 031042 (2019).

40 R. Comin *et al*., Charge order driven by Fermi-arc instability in $Bi_2Sr_{2-x}La_xCuO_{6+\delta}$. *Science* **343**, 390-392 (2014).

41 E. H. da Silva Neto *et al*., Ubiquitous interplay between charge ordering and high-temperature superconductivity in cuprates. *Science* **343**, 393-396 (2014).

42 S. D. Edkins *et al.,* Magnetic field–induced pair density wave state in the cuprate vortex halo. *Science* **364**, 976-980 (2019).

43 Z. Dai, T. Senthil and P. A. Lee, Modeling the pseudogap metallic state in cuprates: quantum disordered pair density wave. arXiv:1906.01656 (31 October 2019).

Figure 1

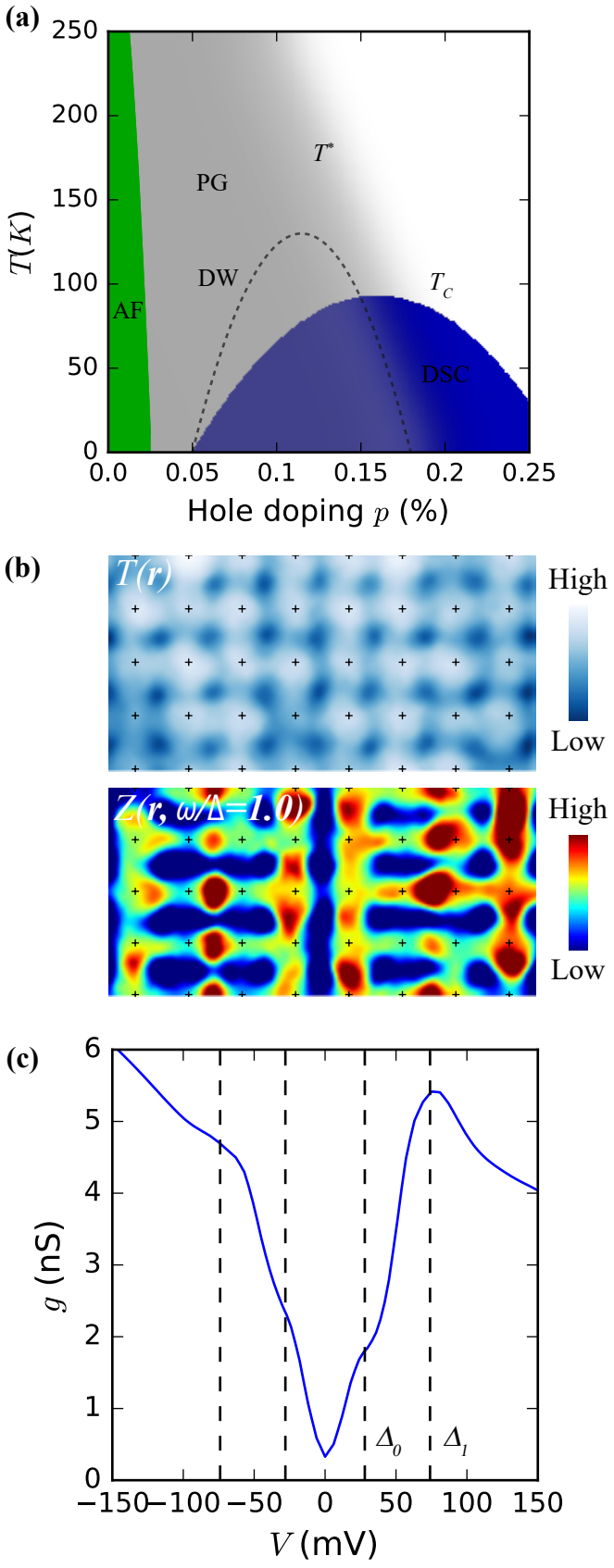
(a)
250
200
150
100
50
0
T(K)
PG
T*
DW
T_c
AF
DSC
0.0
0.05
0.1
0.15
0.2
0.25
Hole doping p (%)
(b)
T(r)
High
Low
Z(r, ω/Δ=1.0)
High
Low
(c)
6
5
4
3
2
1
0
g (nS)
Δ0
Δ1
−150
−100
−50
0
50
100
150
V (mV)

Figure 2

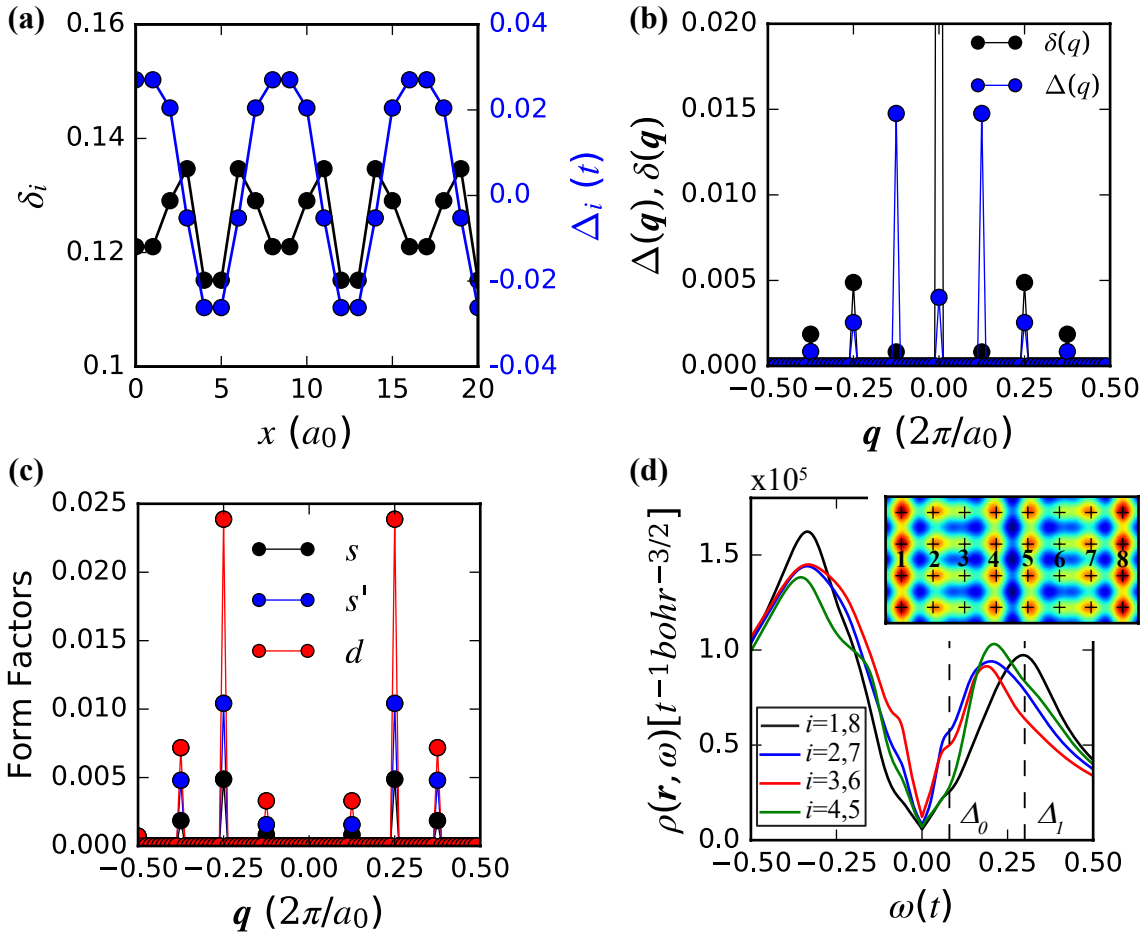
(a)
0.16
0.14
0.12
0.1
δ_i
0.04
0.02
0.0
-0.02
-0.04
Δ_i (t)
0
5
10
15
20
x (a_0)
(b)
0.020
0.015
0.010
0.005
0.000
$\Delta(q), \delta(q)$
$\delta(q)$
$\Delta(q)$
−0.50 −0.25 0.00 0.25 0.50
q ($2\pi/a_0$)
(c)
0.025
0.020
0.015
0.010
0.005
0.000
Form Factors
s
s'
d
−0.50 −0.25 0.00 0.25 0.50
q ($2\pi/a_0$)
(d)
x10^5
1.5
1.0
0.5
0.0
$\rho(r, \omega)[t^{-1}bohr^{-3/2}]$
1 2 3 4 5 6 7 8
i=1,8
i=2,7
i=3,6
i=4,5
Δ_0
Δ_1
−0.50 −0.25 0.00 0.25 0.50
$\omega(t)$

Figure 3

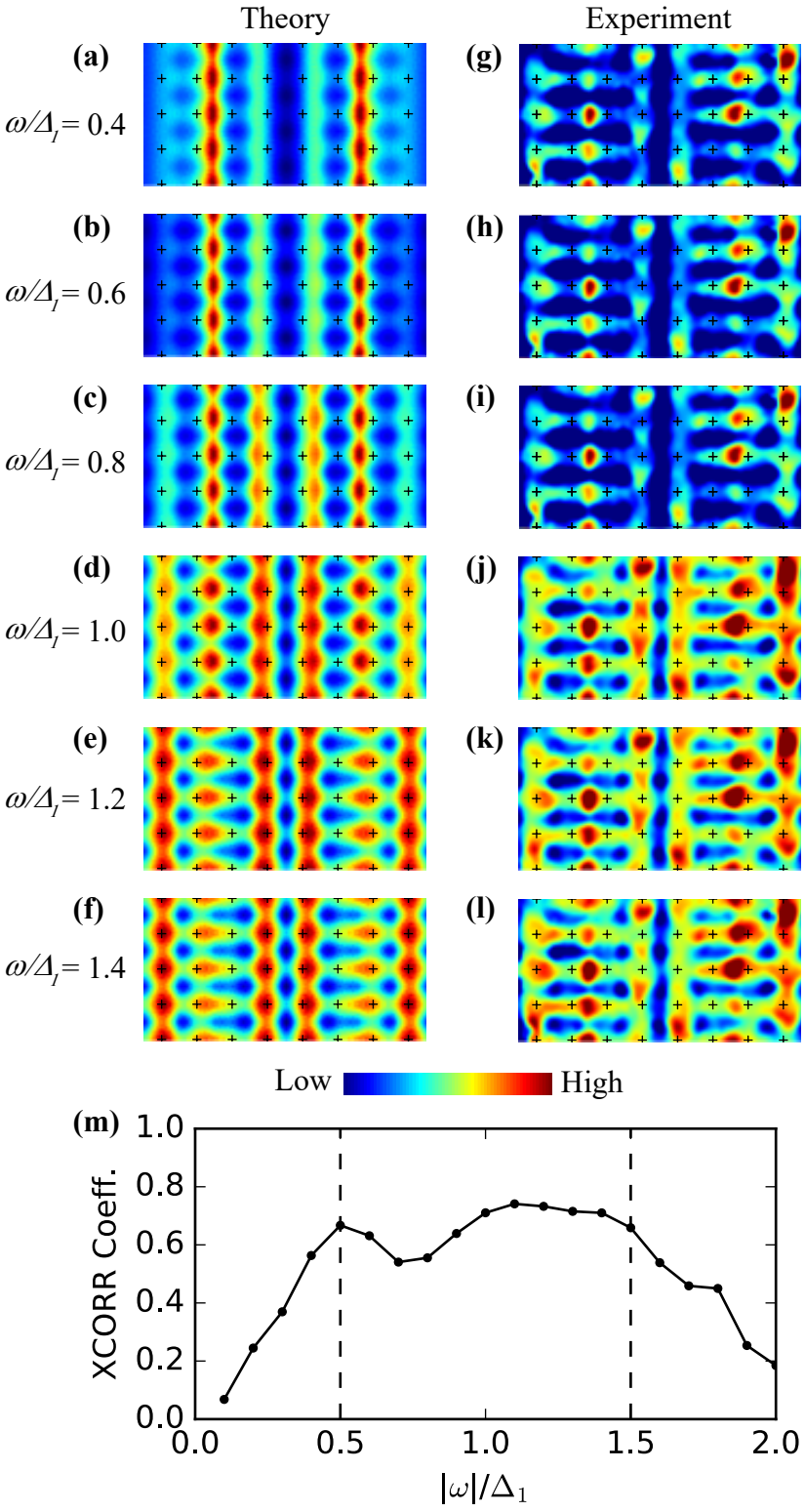
Theory
Experiment
(a)
$\omega/\Delta_1 = 0.4$
(g)
(b)
$\omega/\Delta_1 = 0.6$
(h)
(c)
$\omega/\Delta_1 = 0.8$
(i)
(d)
$\omega/\Delta_1 = 1.0$
(j)
(e)
$\omega/\Delta_1 = 1.2$
(k)
(f)
$\omega/\Delta_1 = 1.4$
(l)
Low
High
(m)
XCORR Coeff.
0.0
0.2
0.4
0.6
0.8
1.0
0.0
0.5
1.0
1.5
2.0
$|\omega|/\Delta_1$

Figure 4

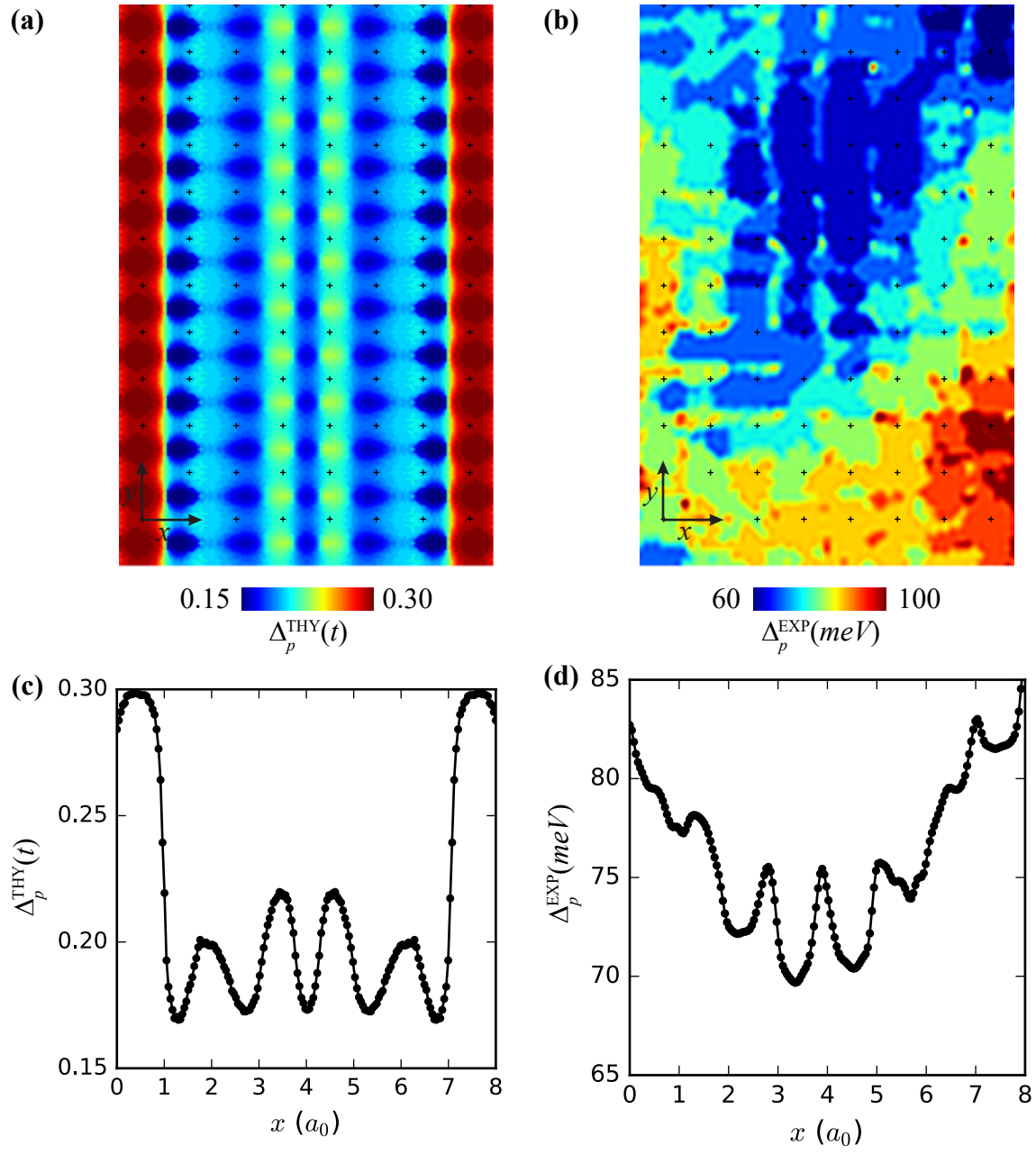
(a)
(b)
0.15
0.30
$\Delta_p^{\mathrm{THY}}(t)$
60
100
$\Delta_p^{\mathrm{EXP}}(meV)$
(c)
(d)
$\Delta_p^{\mathrm{THY}}(t)$
$\Delta_p^{\mathrm{EXP}}(meV)$
$x\ (a_0)$
$x\ (a_0)$

Figure 5